PCCP

ROYAL SOCIETY OF CHEMISTRY

PAPER

View Article Online
View Journal | View Issue

Cite this: *Phys. Chem. Chem. Phys.*, 2025, **27**, 8327

Analyzing spectral distributions of charge transfer character in ensembles: a case study on the reaction center of photosystem II†

Adam Šrut, [a] Sinjini Bhattacharjee, [b] Dimitrios A. Pantazis *[b] and Vera Krewald *[a]

Received 23rd January 2025,
Accepted 25th March 2025

DOI: 10.1039/d5cp00317b

rsc.li/pccp

Understanding the primary charge separation events in Nature's photosynthetic reaction centers is a key step toward harnessing the microscopic processes of light conversion into chemical energy. Despite intense research efforts employing state-of-the-art spectroscopic and theoretical techniques, the precise nature of energy transfer and charge separation events in these systems are still insufficiently understood. Herein, we present a computational approach that enables analysis of the charge transfer character in excited electronic states with inclusion of thermal effects in ensembles. We showcase an application of this approach to the reaction center of photosystem II, focusing on the $Chl_{D1}Pheo_{D1}$ and $P_{D1}P_{D2}$ pairs of pigments. We find that the $Chl_{D1}Pheo_{D1}$ pair is a more likely candidate for the primary charge separation than the $P_{D1}P_{D2}$ pair. Our computational approach is transferable to other biological and man-made charge separation and charge transfer systems.

1. Introduction

The thorough understanding of energy and electron transfer mechanisms in photosynthetic pigment–protein complexes is essential for the knowledge-guided design of synthetic platforms and devices that will drive the energy transition. Photosystem II (PSII) of oxygenic photosynthesis[1] is one of the most important potential blueprints for artificial light-driven charge-separating devices.[2–4] The four chlorophyll and two pheophytin molecules that comprise the reaction center (RC) of PSII (Fig. 1) are able to convert with ultimate efficiency visible light to electron flow, powering water oxidation and plastoquinone reduction.[5–7] Three main factors need to be elucidated for understanding the function of the PSII RC, each factor representing a substantial challenge for both experiment and theory: (a) the electronic structure of the pigments themselves, (b) the influence of the protein environment in terms of structure and electrostatics, and (c) the role that dynamic motion plays in modulating the electronic structure, absorption properties, and function of RC pigments. Since the initial charge separation is intimately tied to the light absorption process, the electronic structure analysis must encompass the ground state and the spectrum of low-lying excited states.

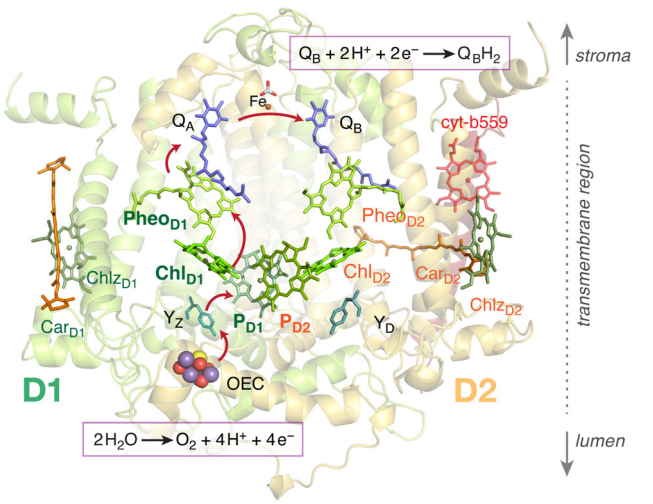

Fig. 1 The chlorophyll and pheophytin pigments comprising the reaction center of PSII. Important additional cofactors of PSII are also indicated. The primary charge separation occurs among pigments of the D1 protein, initiated either within the $Chl_{D1}Pheo_{D1}$ or the $P_{D1}P_{D2}$ pairs, following direct light absorption or excitation energy transfer from intrernal and external light harvesting complexes. The arrows depict the flow of electrons from the donor side (water oxidation) to the acceptor side (plastoquinone reduction).

[a] *TU Darmstadt, Department of Chemistry, Quantum Chemistry, Peter-Grünbegr-Straße, 64287 Darmstadt, Germany E-mail: vera.krewald@tu-darmstadt.de*
[b] *Max-Planck-Institut für Kohlenforschung, Kaiser-Wilhelm-Platz 1, 45470 Mülheim an der Rühr, Germany. E-mail: dimitrios.pantazis@kofo.mpg.de*

† Electronic supplementary information (ESI) available: Further details on system setup and QM/MM calculations; analysis scripts; natural transition orbitals; charge transfer numbers; spectral quantities in adiabatic representation. See DOI: https://doi.org/10.1039/d5cp00317b

Crucial advances have been made toward a reliable description of the electronic structure of chlorophylls using modern quantum chemical methods,[8–11] while the influence of the protein environment on the PSII RC properties and function has also began to be reliably quantified in recent studies using hybrid quantum-mechanics/molecular-mechanics (QM/MM) approaches.[12–15] Initial studies have also begun to consider how the flexibility of the protein environment affects the properties of RC pigments.[16,17] On the other hand, the flexibility of the geometric structures of the pigments themselves is a crucial factor that remains unexplored, in part because the classical force fields used in typical molecular dynamics studies of PSII are not able to correctly sample the conformation flexibility of the photosynthetic macrocycles. This flexibility however can have important implications for the theoretical description of the primary RC function[13] as well as for the charge separation processes that follow the initial photo-initiation.[18–20]

Methods for characterising excited states are well established.[21,22] Specifically, the charge-transfer character of an excited state can be conveniently analysed with electron–hole correlation plots[23] or natural transition orbitals.[24] These methods represent both qualitative and quantitative ways to analyze the wavefunction of an excited state. A distinct challenge, however, is how to perform such analysis in an *ensemble* of distorted geometries, as it will be present in reality due to zero point vibrations, conformational flexibility and other effects. The electronic states will reorder and mix among each other upon distortion of the nuclear coordinates. Each member of the ensemble can thus possess a different set of electronic states. Herein, we present a new way to analyse a thermally populated nuclear ensemble. We solve the issue of reordering and mixing of the electronic states by calculating the electronic properties in a chosen set of reference states.[25,26] Our method is rooted in the determination of wavefunction overlaps and is exemplified with the $Chl_{D1}Pheo_{D1}$ and $P_{D1}P_{D2}$ pairs of Photosystem II. We expect the method to be generally applicable to electron transfer chains in enzymes as well as in synthetic charge-separating systems.

2. Methodology

The fundamental idea of the presented approach is to analyze an ensemble of distorted geometries in a unified basis of electronic states. The ensemble is generated only by sampling the individual pigment pairs in the frozen environment of the protein. The reference states, with respect to which the ensemble is analyzed, are the electronic states at Franck–Condon (FC) geometry. These states are well characterized by means of natural transition orbitals and charge transfer numbers.

At each geometry in the ensemble, wavefunction overlaps of the excited states with the reference states are calculated. These are then collected into an overlap matrix with elements:

$$S_{ij} = \langle \psi_i^{\mathrm{FC}} | \psi_j^{\mathrm{dist}} \rangle \tag{1}$$

where ψ_i^{FC} is the i-th electronic state at the FC geometry and ψ_j^{dist} is the j-th state at the distorted geometry. It is now tempting to assume that any state at the distorted geometry can be described as a linear combination of the states at the FC geometry and *vice versa*. From this assumption it follows that the overlap matrix needs to be orthogonal, which can be demonstrated by employing the resolution of identity:

$$\begin{aligned} 1 &= \left\langle \psi_i^{\mathrm{FC}} | \psi_i^{\mathrm{FC}} \right\rangle \\ &= \left\langle \psi_i^{\mathrm{FC}} \middle| \sum_{j=1}^{N_{\mathrm{states}}} \middle| \psi_j^{\mathrm{dist}} \right\rangle \left\langle \psi_j^{\mathrm{dist}} \middle| \psi_i^{\mathrm{FC}} \right\rangle \\ &= \sum_{j=1}^{N_{\mathrm{states}}} |S_{ij}|^2 \end{aligned} \tag{2}$$

In reality, however, the overlap matrix will deviate from orthogonality $\left(i.e.\ \sum_j |S_{ij}|^2 \neq 1 \right)$ because of the displacement of basis functions, truncation of the wavefunction and interaction with external states.[27] The overlap matrix can be, however, orthogonalized using Löwdin orthogonalization.[27,28] The resulting matrix will then satisfy eqn (2). We further note that in case of extremely large structural changes the calculation of wavefunction overlaps might be too inaccurate and the orthogonalized matrix will deviate too much from the original one.

We wish to use the electronic states at the FC geometry as reference states (or the so-called diabatic basis) in the analysis of the ensemble. The quantity we thus need is the expectation value of a given operator for a system in a reference state $\psi_\alpha^{\mathrm{FC}}$, but at a distorted geometry. The reference state can be written as an expansion of the electronic states at the distorted geometry using the overlap matrix:

$$\left| \psi_\alpha^{\mathrm{FC}} \right\rangle = \sum_{j=1}^{N_{\mathrm{states}}} S_{\alpha j} \left| \psi_j^{\mathrm{dist}} \right\rangle \tag{3}$$

Inserting this expansion into the formula for an expectation value of a Hamiltonian operator $\hat{H}$ for a system in a state $|\psi_\alpha^{\mathrm{FC}}\rangle$ will result in:

$$\begin{aligned} E_\alpha &= \left\langle \psi_\alpha^{\mathrm{FC}} \middle| \hat{H} \middle| \psi_\alpha^{\mathrm{FC}} \right\rangle \\ &= \sum_{i=1}^{N_{\mathrm{states}}} \sum_{j=1}^{N_{\mathrm{states}}} S_{\alpha i} S_{\alpha j} \left\langle \psi_i^{\mathrm{dist}} \middle| \hat{H} \middle| \psi_j^{\mathrm{dist}} \right\rangle \\ &= \sum_{i=1}^{N_{\mathrm{states}}} \sum_{j=1}^{N_{\mathrm{states}}} S_{\alpha i} S_{\alpha j} H_{ij} \end{aligned} \tag{4}$$

where H_{ij} is an element of a matrix representation of the Hamiltonian in the basis of electronic states of the distorted geometry. Because there is no potential coupling between these (adiabatic) states, the Hamiltonian matrix will be diagonal and the final expression can be simplified even further:

$$E_\alpha = \sum_{i=1}^{N_{\mathrm{states}}} |S_{\alpha i}|^2 H_{ii} \tag{5}$$

This approach is conceptually similar to the local diabatization scheme frequently used in non-adiabatic dynamics.[29,30] Notably, this idea was recently employed for parameterization

of vibronic coupling Hamiltonian for non-adiabatic quantum dynamics of the PSII RC.[31]

The transition dipole moments and charge transfer characters describe the transition between the ground state and an excited state which needs to be taken into account in the diabatization procedure. To make the diabatization of these quantities possible we are going to assume that the electronic ground state remains unaffected by molecular vibrations, *i.e.* $|\psi_{GS}^{FC}\rangle = |\psi_{GS}^{dist}\rangle$. This is a reasonable assumption if the ground state has a closed shell configuration and is energetically well separated from the excited states which precludes any mutual mixing. The magnitude of the transition dipole moment ($|\vec{\mu}_{GS\to\alpha}|^2$) cannot be converted directly into the new basis. First, the individual Cartesian components have to be calculated in the new basis. For example, the *x*-component is calculated as:

$$\begin{aligned}\mu_{x,GS\to\alpha} &= \sum_{i=1}^{N_{states}} S_{\alpha i}\langle\psi_{GS}^{dist}|\hat{\mu}_x|\psi_i^{dist}\rangle \\ &= \sum_{i=1}^{N_{states}} S_{\alpha i}\mu_{x,GS\to i}\end{aligned} \tag{6}$$

The magnitude of the transition dipole moment vector is then computed from its components:

$$|\vec{\mu}_{GS\to\alpha}|^2 = {\mu_{x,GS\to\alpha}}^2 + {\mu_{y,GS\to\alpha}}^2 + {\mu_{z,GS\to\alpha}}^2 \tag{7}$$

The transition dipole moment is converted into oscillator strength, which can be used to compute an absorption spectrum, according to:

$$f_{GS\to\alpha} = \frac{2m_e E_\alpha}{3\hbar^2 e^2}|\vec{\mu}_{GS\to\alpha}|^2 \tag{8}$$

where m_e is the mass of the electron, e is the elementary charge, $\hbar$ is reduced Planck constant and E_α is the diabatic excitation energy of state α from eqn (5).

For the charge transfer numbers, the problem is essentially similar to the computation of excited state characters of spin-mixed states, described in ref. 32 One can thus write:

$$\Omega_\alpha = \sum_{i=1}^{N_{states}} |S_{\alpha i}|^2 \Omega_i^{dist} \tag{9}$$

where Ω_α is an amount of charge transfer character for a transition from the ground state to an excited state α and Ω_i^{dist} is the same quantity for state i at the distorted geometry.

The absorption spectra, densities of states and charge transfer densities were calculated by collecting the corresponding quantities for each electronic state and distorted geometry along the energy axis into a line spectrum. This spectrum is subsequently broadened *via* a convolution with a Gaussian. The formula for the absorption spectrum of a single electronic state is:

$$\sigma_\alpha(E) = \int_0^\infty \left[\sum_{j=1}^{N_{geoms}} f_{\alpha,j}\cdot\delta(E' - E_{\alpha,j})\right] \cdot e^{-\left(\frac{E-E'}{FWHM}\cdot 2\sqrt{\ln 2}\right)^2} dE' \tag{10}$$

where δ is the Dirac delta function, FWHM is the full width at half maximum (0.1 eV was used in this work), $f_{\alpha,j}$ and $E_{\alpha,j}$ are oscillator strength and excitation energy of electronic state α at j-th geometry in the ensemble, respectively. For the total absorption spectrum, an additional sum over the electronic states has to be added. Calculation of the charge transfer density only requires the substitution of $f_{\alpha,j}$ by the charge transfer character of state α at j-th geometry, $\Omega_{\alpha,j}$. The density of states is calculated by setting all $f_{\alpha,j}$ to one.

3. Computational details

The molecular dynamics simulations of PSII were unchanged from the previous studies.[11,13,33] The model of the PSII is based on the crystal structure of *T. vulcanus* (3WU2.pdb).[34] A detailed description is provided in the ESI.†

QM/MM geometry optimizations for the reaction center pigments ($Chl_{D1}Pheo_{D1}$, $P_{D1}P_{D2}$) were performed using the PBE functional,[35] def2-TZVP basis set[36] and electrostatic embedding in ORCA 5.0.[37] Using a GGA functional for optimizations of chlorophylls and related systems is known to provide reasonable structures while maintaining a moderate computational cost.[8,10,12] Optimized structures are depicted in Fig. 2a and b. Frequency calculations were performed *in vacuo* for the optimized pigment pairs on the PBE/def2-TZVP level. Further details are given in the ESI.†

The sampling of the thermal ensemble was achieved with the Wigner sampling method at 300 K utilizing the frequency calculation described above. The implementation in the SHARC package[38] was used. Modes with imaginary frequencies or frequencies lower than 100 cm^{-1} were discarded from the sampling procedure. An ensemble of 700 distorted geometries was generated for further single-point calculations. The ensembles are shown in Fig. 2c and d. The sampled geometries were

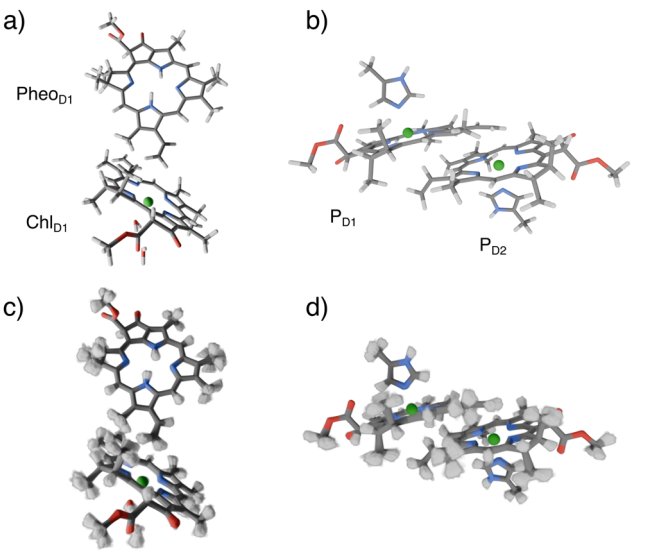

Fig. 2 QM/MM optimized structures of the $Chl_{D1}Pheo_{D1}$ and $P_{D1}P_{D2}$ pairs (a) and (b) and their sampled geometries (c) and (d) at 300 K using a Wigner sampling method.

then inserted into the frozen protein matrix. We note that additional sampling of the protein environment is conceivable but it would significantly increase the number and complexity of the calculations in practice. For these reasons we will not explore this effect here.

Excited states at each geometry in the ensemble were calculated with the time-dependent density functional theory (TD-DFT) utilizing the TURBOMOLE package.[39] The range-separated density functional ωB97X-V[40] was employed together with the def2-TZVP basis set.[36] The calculations employed the resolution of identity approximation,[41] an integration grid of size m3,[42] and the convergence criterion of the self-consistent field method was set to $10^{-8}E_h$. Seven excited states were calculated for each geometry of the ensemble without the Tamm–Dancoff approximation. The protein environment was modeled as point charges.

Charge transfer numbers were computed using the TheoDORE package.[43] The molecule was divided into two fragments corresponding to the two monomers, *i.e.* Chl_{D1} and $Pheo_{D1}$, or P_{D1} and P_{D2}. Since the TD-DFT calculations were performed without the Tamm–Dancoff approximation which employs different normalization of the excitation vector ($\boldsymbol{X}$), the charge transfer numbers for each state needed to be renormalized to sum up to one.

The overlaps of the wavefunctions between the Franck–Condon and distorted geometries were computed with the WFoverlap program,[27] which is a part of the SHARC package.[38] The program requires overlaps of atomic orbitals (AOs) between the two geometries, molecular orbitals (MOs), and electronic states as expansions of Slater determinants. Using the MO coefficients of the two wavefunctions, the AO overlaps are transformed to the MO overlaps and subsequently to the overlaps between the determinants.[27]

The overlap matrix between the AO bases was computed using the ORCA[37] orca_fragovl module. The two gbw files for both geometries required as an input can be generated for example with a Hartree–Fock calculation with no SCF iterations and the same basis set as the TD-DFT calculations. The output of orca_fragovl was then reformatted for the WFoverlap program. The 1s orbitals of non-hydrogen atoms were discarded from the overlap calculation.

The TD-DFT states are described as expansions of singly excited determinants. The expansion coefficients are written into the sing_a file generated by TURBOMOLE. They need to be reformatted for the WFoverlap program.

The studied systems contain around 3000 orbitals and have hundreds of thousands of possible single excitations. Calculating a wavefunction overlap would thus require determining roughly 10^{11} determinant pairs. A calculation of this magnitude would be too demanding regarding both CPU time and memory requirements. To reduce the number of singly excited determinants we employed a commonly used truncation of the wavefunction.[27] The squared expansion coefficients were first sorted in descending order. Then, the configurations were taken from the ordered list to the overlap calculation until the sum of the squared expansion coefficient reached a threshold of 0.996 for $Chl_{D1}Pheo_{D1}$ pair and 0.994 for $P_{D1}P_{D2}$ pair. In this way, the number of determinants was reduced to only several thousands which led to a significant reduction of computational costs while maintaining accuracy.

The analysis scripts can be freely accessed in an open-source format at: **https://git.rwth-aachen.de/ak-krewald/nuclear_ensemble_analysis**. Details on their usage are provided in the ESI.†

4. Results and discussion

4.1. State mixing and reordering in nuclear ensembles

To calculate the total absorption spectrum for the full ensemble it would be straightforward to sum over the individual spectra of each member of the ensemble. Similarly, the densities of states (DOS) and densities of charge transfer (CT) character can be easily accessed. However, for a more detailed analysis it is of interest to deconvolve the properties of the average spectrum into the contributions of the individual electronic states. Examining the characters and contributions of individual states in each member of an ensemble is not straightforward because the electronic structure at each distorted geometry will differ. This is caused by a reordering of the excited electronic states or by a mixing of their characters. In other words, the electronic states of the distorted geometries are not going to be in 1 : 1 correspondence with the states at the optimized geometry. The physical origins of reordering and mixing of the excited states can be traced to the presence of conical intersections and the Herzberg–Teller effect,[44] respectively.

For the discussion of charge separation in light harvesting and energy conversion devices, it is of central importance to understand at which energies the charge separation takes place and which electronically excited states are responsible for this process. To facilitate this analysis, we chose a set of well-defined reference states and use these as a basis for the analysis of spectral properties. An intuitive and meaningful choice of reference states are the electronic states at the optimized geometry, *i.e.* the FC geometry. We analyse their characters *via* charge transfer numbers[43] (see Fig. 3) and natural transition orbitals (see ESI†).

The reference states are characterized in Fig. 3 *via* the charge transfer numbers. For the $Chl_{D1}Pheo_{D1}$ pair (Fig. 3a), we find three charge transfer states at 1.64, 2.15 and 2.80 eV. They correspond to the first, third and seventh state, and have pure $Chl_{D1} \rightarrow Pheo_{D1}$ CT character. For the $P_{D1}P_{D2}$ pair (Fig. 3b), we also find three CT states, here at 2.90, 3.19 and 3.35 eV, which correspond to the fifth, sixth and seventh states at the FC point. These states have either $P_{D1} \rightarrow P_{D2}$ or $P_{D2} \rightarrow P_{D1}$ character mixed with local excitation character.

To assess the state characters at the distorted geometries, we define a transformation between the reference states and the electronic states at a particular distorted geometry *via* wavefunction (WF) overlaps[27,45] of the two sets of states. Each electronic state at a distorted geometry is expressed as a linear combination of the reference states. The properties of the excited states in the distorted geometries are calculated accordingly.

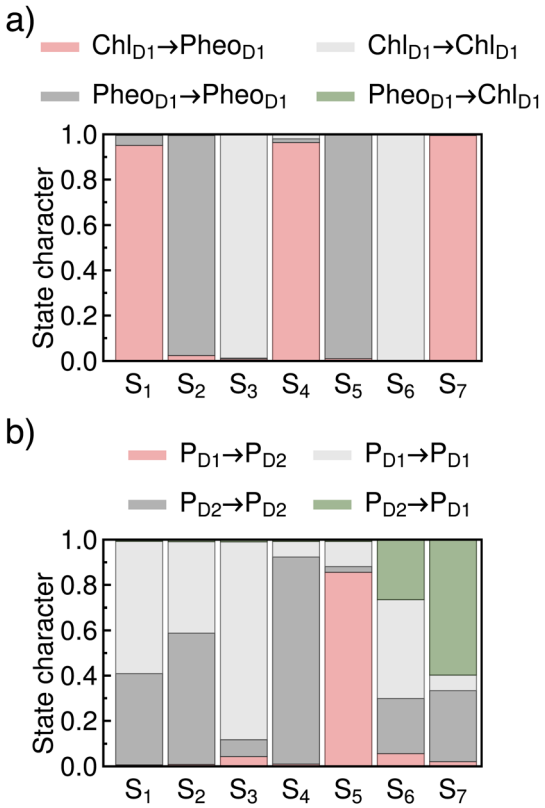

Fig. 3 Characterization of the excited states *via* their charge transfer numbers. (a) Excited state characters of $Chl_{D1}Pheo_{D1}$ pair at the FC geometry. (b) Excited state characters of $P_{D1}P_{D2}$ pair at the FC geometry.

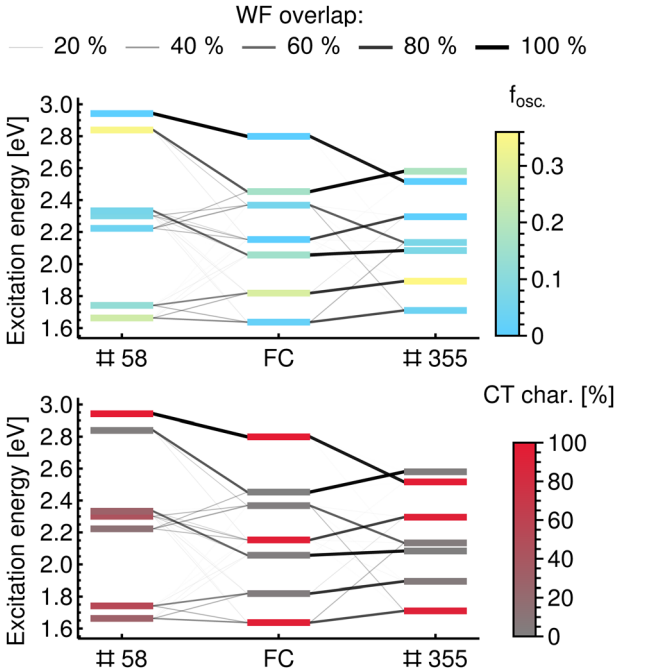

Fig. 4 Illustration of mixing and reordering of excited states using wavefunction overlaps with the Franck–Condon geometry as a reference for the $Chl_{D1}Pheo_{D1}$ pair. Geometry #58 represents an example of the mixing of states, while geometry #355 illustrates reordering. States are coloured by the oscillator strength from the ground state in the upper panel and by the portion of the Chl_{D1} → $Pheo_{D1}$ CT character in the lower panel.

In Fig. 4 we show the CT characters and oscillator strengths for the reference states of the $Chl_{D1}Pheo_{D1}$ pair at the FC geometry. And the effects of the vibrational distortions on the electronic states are illustrated for two representative geometries of the ensemble, geometry #58 and geometry #355.

In geometry #58, the excited states arise from the mixing of state characters at the FC geometry. This means that an electronic state of the distorted geometry has similar WF overlap values with two or more states at the reference geometry, as is illustrated with connecting lines of different weights in Fig. 4. As a result, the excited states of this geometry have intermediate values of CT character, in contrast to the reference states that have CT character of either close to 0% (local excitations) or 100% (CT excitations). In contrast, in geometry #355 the excited states are formed mainly by reordering of the reference states. This means that each excited state at a distorted geometry has significant overlap with only one of the reference states. This reordering is shown in Fig. 4 by one dominant line connecting the states at the distorted geometry with the reference states at the FC geometry. As a result, the excited states are also either CT states or locally excited ones (*i.e.* CT character close to 0 or 100%); only their order is different than at the FC geometry.

In conclusion, relating the excited states between a distorted geometry in the ensemble and FC geometry or between two distorted geometries of the ensemble simply based on their energetic ordering cannot provide detailed insight into the properties of the ensemble. This is exemplified Fig. 4, where a change in geometry by a vibrational distortion leads to a different set of excited electronic states.

4.2. Analysis with the reference states

Electronic states in a nuclear ensemble need to be characterized in a unified basis to suppress their mixing and reordering upon change in the nuclear configuration. Herein, we propose to use the electronic states at the FC geometry as the reference states and express each electronic state at a distorted geometry of the ensemble as a linear combination of them utilizing the wavefunction overlaps. The workflow is described in the Methodology section. In Fig. 5, we illustrate the proposed method schematically.

Fig. 5a shows the conventional calculation of a spectral feature (absorption spectrum, density of states, *etc.*) where the electronic states are simply ordered by their energies. The resulting composition of the first peak in the spectrum is a mixture of two electronic states with different characters. When the analysis in the basis of the reference states as proposed here is introduced, the excited states become ordered by their character, see Fig. 5b. The spectral features are now comprised only of excited states with the same character. In this way, the true distribution of the density of a single electronic state (or any other property) along the energy axis can be extracted from a nuclear ensemble.

While the results presented in this work are based on TD-DFT calculations, an extension to wavefunction methods is conceivable and not hindered by any fundamental limitations.

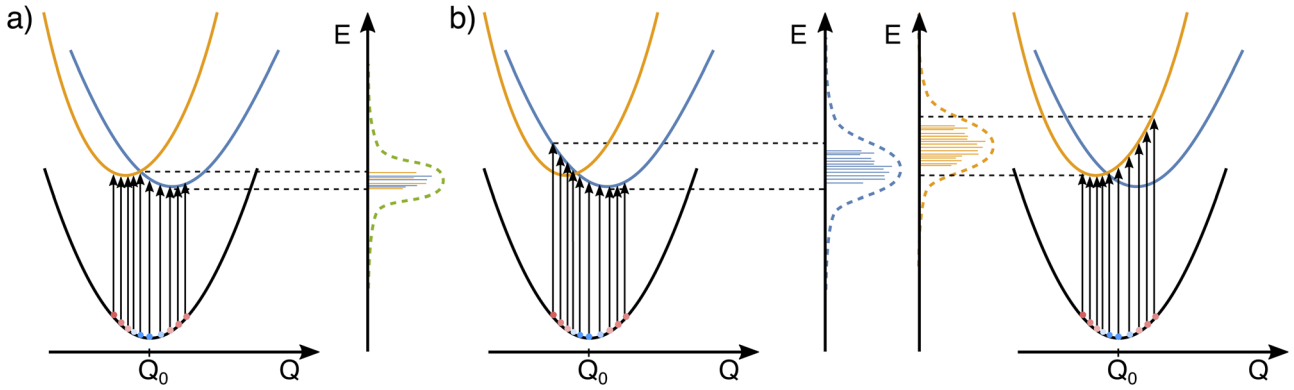

Fig. 5 Schematic description of the presented methodology for analyzing a nuclear ensemble in a unified basis of electronic states. (a) The electronic states are ordered by their energies and the spectral feature of a first excited state is a mix of two state characters. (b) The electronic states are ordered by their character and the spectral features of both excited states are composed of the states that preserve character.

This will be connected with a higher computational cost when computing the wavefunction overlaps, but the true bottleneck will lie in reformatting the electronic states to expansions of Slater determinants. Efforts in this direction were recently presented in conjunction with different quantum chemistry packages.[27,46,47]

4.3. Reaction center in photosystem II

Applying the presented methodology to the thermally populated ensembles of the PSII pigments $Chl_{D1}Pheo_{D1}$ and $P_{D1}P_{D2}$ means that we will be able to correctly discuss the contributions of the individual states to the DOS, to the absorption spectra, and to the densities of CT character.

For the $Chl_{D1}Pheo_{D1}$ pair, the distribution of the density of $Chl_{D1} \rightarrow Pheo_{D1}$ CT character is almost uniform, see Fig. 6a. The CT character is predominantly due to three excited states, S_1, S_4 and S_7. Importantly, the lowest-energy state has CT character (S_1 state). This means that for any type of excitation, either directly by visible light or by energy transfer from the antenna system, the $Chl_{D1}Pheo_{D1}$ pair is expected to relax by internal conversion into this charge separated state. The absorption spectrum of $Chl_{D1}Pheo_{D1}$ pair is plotted in Fig. 6b. It covers almost the entire visible spectrum with the highest absorption at the low energy end. The pair can thus act as a light absorber itself, *e.g. via* S_2, and then relax into the charge separated state S_1.

For the $P_{D1}P_{D2}$ pair, charge transfer states ($P_{D1} \rightarrow P_{D2}$, $P_{D2} \rightarrow P_{D1}$) appear only at the high energy end of the spectrum, see Fig. 6c. Notably, no CT character occurs for the lowest lying excited states. This means that any energy that the $P_{D1}P_{D2}$ pair receives, radiatively or non-radiatively, would not be funneled into a charge separated state upon internal conversion. This behaviour is in a strong contrast to the $Chl_{D1}Pheo_{D1}$ pair.

The properties of the $P_{D1}P_{D2}$ pair as a light absorber also differ from $Chl_{D1}Pheo_{D1}$ pair. The highest absorption is observed only at the red and blue ends of the visible spectrum, see Fig. 6d, while in the energy window from 2.1 to 2.7 eV the $P_{D1}P_{D2}$ pair absorbs only weakly. The pair thus appears to

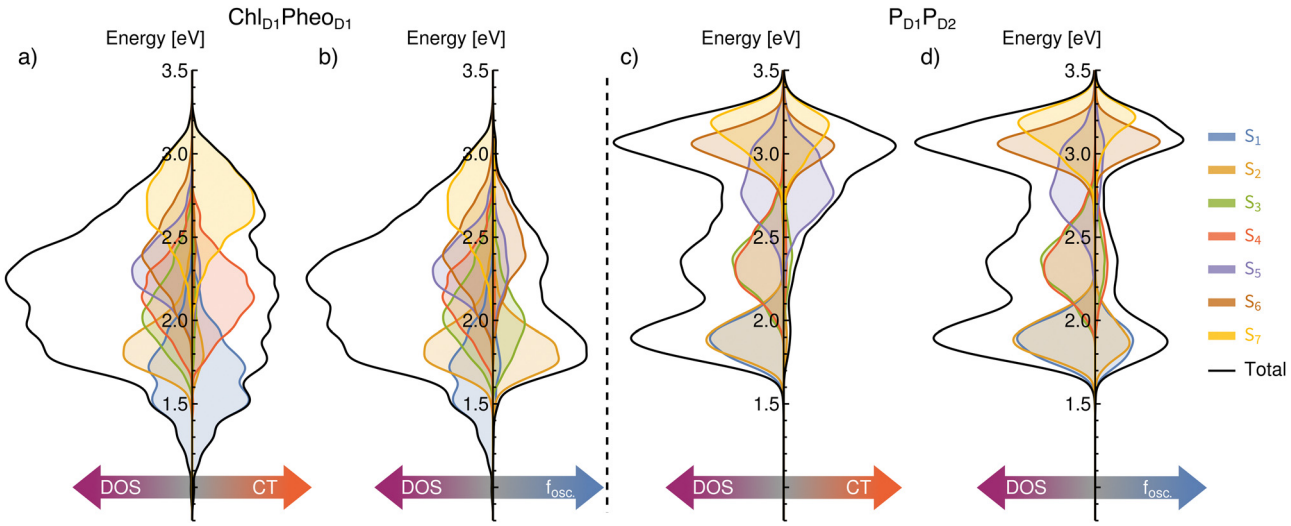

Fig. 6 Spectral characteristics of $Chl_{D1}Pheo_{D1}$ and $P_{D1}P_{D2}$ pairs. (a) DOS and density of the $Chl_{D1} \rightarrow Pheo_{D1}$ CT character. (b) DOS and absorption spectrum in $Chl_{D1}Pheo_{D1}$ pair. (c) DOS and density of $P_{D1} \rightarrow P_{D2}$ and $P_{D2} \rightarrow P_{D1}$ CT characters. (d) DOS and absorption spectrum in $P_{D1}P_{D2}$ pair.

utilise visible light in a not very efficient manner, supporting the argument that the excitation of the $P_{D1}P_{D2}$ pair happens *via* an energy transfer.

Looking at the interplay of the two pairs as reflected by our findings, we note that the DOS of $Chl_{D1}Pheo_{D1}$ extends almost to 1 eV at the low energy end, whereas the DOS of the $P_{D1}P_{D2}$ pair does not go below 1.5 eV. This implies that energy transfer from $P_{D1}P_{D2}$ to $Chl_{D1}Pheo_{D1}$ might be possible, allowing for charge separation in the S_1 state of $Chl_{D1}Pheo_{D1}$ pair at the bottom of the energy funnel.

Pathways for the charge separation often involve both pigment pairs together, which leads to multiple possible charge separated species (radical pairs) within the D1 branch, with the exact identities of electron transfer intermediates remaining under investigation.[13,17,18,48–52] Although the requisite calculations at the present level of theory would be computationally very demanding, extending the presented methodology to the whole tetramer is in principle possible and conceptually straightforward.

5. Conclusion

Herein, we present an ensemble-based computational approach that accounts for the influence of zero-point energy and finite temperature on the electronic states of pigments in PSII. Furthermore, by utilizing wavefunction overlaps with a set of reference states, the mixing and reordering of electronic states in the ensemble is resolved, which provides insights into individual state contributions to the spectral properties like the DOS, the density of CT character or the absorption spectrum. Our method is transferable to any biological or artificial system in which charge-separation or charge transfer can occur (*i.e.* systems with well-defined donor and acceptor sites).

Our results suggest that the ability of the $Chl_{D1}Pheo_{D1}$ pair to create a charge separated species is much greater than of the $P_{D1}P_{D2}$ pair. Intriguingly, the $Chl_{D1}Pheo_{D1}$ pair exhibits a uniform distribution of $Chl_{D1} \rightarrow Pheo_{D1}$ CT character over the entire visible spectrum. Moreover, the lowest lying excited state is a CT state, which suggests a possible stabilization of the charge separated species after vibrational cooling and internal conversion. In contrast, CT character is only found at the high energy end of the visible spectrum of the $P_{D1}P_{D2}$ pair. Internal conversion after an excitation would thus produce only locally excited states. The present results therefore provide independent support to the mechanistic scenario where the $Chl_{D1}Pheo_{D1}$ pair is the actual ''special pair'' for the primary charge separation in PSII. This conclusion contrasts with interpretations proposed in some experimental studies that favor initial charge separation within the $P_{D1}P_{D2}$ pair or implicate Chl_{D1} as acceptor,[51,53,54] but is aligned with the intepretations reached by several other studies,[19,55,56] as well as with recent multiscale theoretical investigations of the RC.[11–13,16,17]

In terms of future perspectives, we note that our results can be used to parameterize model exciton Hamiltonians for open quantum system simulations to reconstruct time-resolved or two-dimensional spectra,[20,57–59] an approach that would complement other recent efforts in this direction.[31] Most importantly, the approach demonstrated here for the charge-separating pigment assembly of oxygenic photosynthesis can be applied directly to synthetic systems, leading to a deeper understanding of the structural factors—and, hence, identification of design principles—that control the initiation of electron transfer cascades in natural and artificial photosynthesis.

Data availability

The data supporting this article have been included as part of the ESI.† The analysis scripts are freely available in an open-source format at: https://git.rwth-aachen.de/ak-krewald/nuclear_ensemble_analysis.

Conflicts of interest

There are no conflicts to declare.

Acknowledgements

The authors thank Felix Plasser for insightful discussions. D. A. P. and S. B. gratefully acknowledge support by the Max Planck Society. S. B. thanks the International Max Planck Research School on Reactive Structure Analysis for Chemical Reactions (IMPRS-RECHARGE) for support. A. S. thanks the Merck'sche Gesellschaft für Kunst und Wissenschaft e.V. for financial support. The authors gratefully acknowledge the computing time provided to them on the high-performance computer Lichtenberg at the NHR Center NHR4CES at TU Darmstadt. This is funded by the German Federal Ministry of Education and Research (BMBF) and the Hessian Ministry of Science and Research, Art and Culture (HMWK). Open Access funding provided by the Max Planck Society.

Notes and references

1 R. E. Blankenship, *Molecular Mechanisms of Photosynthesis*, Wiley, Chichester, 3rd edn, 2021, pp. 352.
2 M. R. Wasielewski, *Chem. Rev.*, 1992, **92**, 435–461.
3 H. Dau and I. Zaharieva, *Acc. Chem. Res.*, 2009, **42**, 1861–1870.
4 L. Hammarström, *Acc. Chem. Res.*, 2015, **48**, 840–850.
5 R. Croce, R. v Grondelle, H. v Amerongen and I. v Stokkum, *Light Harvesting in Photosynthesis*, Taylor & Francis/CRC Press, Boca Raton, 2018.
6 D. Shevela, J. F. Kern, G. Govindjee and J. Messinger, *Photosynth. Res.*, 2023, **156**, 279–307.
7 R. Croce and H. van Amerongen, *Nat. Chem. Biol.*, 2014, **10**, 492–501.
8 A. Sirohiwal, R. Berraud-Pache, F. Neese, R. Izsák and D. A. Pantazis, *J. Phys. Chem. B*, 2020, **124**, 8761–8771.
9 A. Sirohiwal, F. Neese and D. A. Pantazis, *J. Chem. Theory Comput.*, 2021, **17**, 1858–1873.

10 A. Sirohiwal and D. A. Pantazis, *Phys. Chem. Chem. Phys.*, 2021, **23**, 24677–24684.
11 M. Drosou, S. Bhattacharjee and D. A. Pantazis, *J. Chem. Theory Comput.*, 2024, **20**, 7210–7226.
12 A. Sirohiwal, F. Neese and D. A. Pantazis, *J. Am. Chem. Soc.*, 2020, **142**, 18174–18190.
13 A. Sirohiwal and D. A. Pantazis, *Acc. Chem. Res.*, 2023, **56**, 2921–2932.
14 D. Narzi, D. Bovi, P. De Gaetano and L. Guidoni, *J. Am. Chem. Soc.*, 2016, **138**, 257–264.
15 A. Forde, S. Maity, V. M. Freixas, S. Fernandez-Alberti, A. J. Neukirch, U. Kleinekathöfer and S. Tretiak, *J. Phys. Chem. Lett.*, 2024, **15**, 4142–4150.
16 A. Sirohiwal and D. A. Pantazis, *Angew. Chem., Int. Ed.*, 2022, **61**, e202200356.
17 M. Capone, A. Sirohiwal, M. Aschi, D. A. Pantazis and I. Daidone, *Angew. Chem., Int. Ed.*, 2023, **62**, e202216276.
18 H. H. Nguyen, Y. Song, E. L. Maret, Y. Silori, R. Willow, C. F. Yocum and J. P. Ogilvie, *Sci. Adv.*, 2023, **9**, eade7190.
19 Y. Yoneda, E. A. Arsenault, S.-J. Yang, K. Orcutt, M. Iwai and G. R. Fleming, *Nat. Commun.*, 2022, **13**, 2275.
20 H.-G. Duan, V. I. Prokhorenko, E. Wientjes, R. Croce, M. Thorwart and R. J. D. Miller, *Sci. Rep.*, 2017, **7**, 12347.
21 F. Plasser, M. Wormit and A. Dreuw, *J. Chem. Phys.*, 2014, **141**, 024106.
22 F. Plasser, S. A. Bäppler, M. Wormit and A. Dreuw, *J. Chem. Phys.*, 2014, **141**, 024107.
23 F. Plasser and H. Lischka, *J. Chem. Theory Comput.*, 2012, **8**, 2777–2789.
24 R. L. Martin, *J. Chem. Phys.*, 2003, **118**, 4775–4777.
25 H. Tamura, *J. Phys. Chem. A*, 2016, **120**, 9341–9347.
26 Y. Xie, S. Jiang, J. Zheng and Z. Lan, *J. Phys. Chem. A*, 2017, **121**, 9567–9578.
27 F. Plasser, M. Ruckenbauer, S. Mai, M. Oppel, P. Marquetand and L. González, *J. Chem. Theory Comput.*, 2016, **12**, 1207–1219.
28 G. Granucci, M. Persico and A. Toniolo, *J. Chem. Phys.*, 2001, **114**, 10608–10615.
29 F. Plasser, G. Granucci, J. Pittner, M. Barbatti, M. Persico and H. Lischka, *J. Chem. Phys.*, 2012, **137**, 22A514.
30 G. Granucci, M. Persico and A. Toniolo, *J. Chem. Phys.*, 2001, **114**, 10608–10615.
31 H. Tamura, K. Saito and H. Ishikita, *Chem. Sci.*, 2021, **12**, 8131–8140.
32 S. Mai, F. Plasser, J. Dorn, M. Fumanal, C. Daniel and L. González, *Coord. Chem. Rev.*, 2018, **361**, 74–97.
33 S. Bhattacharjee, S. Arra, I. Daidone and D. A. Pantazis, *Chem. Sci.*, 2024, **15**, 7269–7284.
34 Y. Umena, K. Kawakami, J.-R. Shen and N. Kamiya, *Nature*, 2011, **473**, 55–60.
35 J. P. Perdew, K. Burke and M. Ernzerhof, *Phys. Rev. Lett.*, 1996, **77**, 3865–3868.
36 F. Weigend and R. Ahlrichs, *Phys. Chem. Chem. Phys.*, 2005, **7**, 3297–3305.
37 F. Neese, *WIREs Comput. Mol. Sci.*, 2022, **12**, 1–15.
38 S. Mai, D. Avagliano, M. Heindl, P. Marquetand, M. F. S. J. Menger, M. Oppel, F. Plasser, S. Polonius, M. Ruckenbauer, Y. Shu, D. G. Truhlar, L. Zhang, P. Zobel and L. González, *SHARC3.0: Surface Hopping Including Arbitrary Couplings – Program Package for Non-Adiabatic Dynamics*, 2023, **https://sharc-md.org/**.
39 S. G. Balasubramani, G. P. Chen, S. Coriani, M. Diedenhofen, M. S. Frank, Y. J. Franzke, F. Furche, R. Grotjahn, M. E. Harding, C. Hättig, A. Hellweg, B. Helmich-Paris, C. Holzer, U. Huniar, M. Kaupp, A. Marefat Khah, S. Karbalaei Khani, T. Müller, F. Mack, B. D. Nguyen, S. M. Parker, E. Perlt, D. Rappoport, K. Reiter, S. Roy, M. Rückert, G. Schmitz, M. Sierka, E. Tapavicza, D. P. Tew, C. van Wüllen, V. K. Voora, F. Weigend, A. Wodyński and J. M. Yu, *J. Chem. Phys.*, 2020, **152**, 184107.
40 N. Mardirossian and M. Head-Gordon, *Phys. Chem. Chem. Phys.*, 2014, **16**, 9904–9924.
41 F. Weigend, *Phys. Chem. Chem. Phys.*, 2006, **8**, 1057.
42 O. Treutler and R. Ahlrichs, *J. Chem. Phys.*, 1995, **102**, 346–354.
43 F. Plasser, *J. Chem. Phys.*, 2020, **152**, 084108.
44 W. Domcke, H. Köppel and L. S. Cederbaum, *Mol. Phys.*, 1981, **43**, 851–875.
45 H.-T. Chen, J. Chen, D. V. Cofer-Shabica, Z. Zhou, V. Athavale, G. Medders, M. F. S. J. Menger, J. E. Subotnik and Z. Jin, *J. Chem. Theory Comput.*, 2022, **18**, 3296–3307.
46 G. Cárdenas and J. J. Nogueira, *Int. J. Quantum Chem.*, 2021, **121**, 26533.
47 A. Loreti, V. M. Freixas, D. Avagliano, F. Segatta, H. Song, S. Tretiak, S. Mukamel, M. Garavelli, N. Govind and A. Nenov, *J. Chem. Theory Comput.*, 2024, **20**, 4804–4819.
48 E. Romero, I. H. Van Stokkum, V. I. Novoderezhkin, J. P. Dekker and R. Van Grondelle, *Biochemistry*, 2010, **49**, 4300–4307.
49 V. I. Novoderezhkin, E. Romero, J. P. Dekker and R. van Grondelle, *ChemPhysChem*, 2011, **12**, 681–688.
50 T. Renger and E. Schlodder, *J. Photochem. Photobiol., B*, 2011, **104**, 126–141.
51 I. V. Shelaev, F. E. Gostev, V. A. Nadtochenko, A. Y. Shkuropatov, A. A. Zabelin, M. D. Mamedov, A. Y. Semenov, O. M. Sarkisov and V. A. Shuvalov, *Photosynth. Res.*, 2008, **98**, 95–103.
52 Y. Silori, R. Willow, H. H. Nguyen, G. Shen, Y. Song, C. J. Gisriel, G. W. Brudvig, D. A. Bryant and J. P. Ogilvie, *J. Phys. Chem. Lett.*, 2023, **14**, 10300–10308.
53 I. V. Shelaev, F. E. Gostev, M. I. Vishnev, A. Y. Shkuropatov, V. V. Ptushenko, M. D. Mamedov, O. M. Sarkisov, V. A. Nadtochenko, A. Y. Semenov and V. A. Shuvalov, *J. Photochem. Photobiol., B*, 2011, **104**, 44–50.
54 E. Romero, R. Augulis, V. I. Novoderezhkin, M. Ferretti, J. Thieme, D. Zigmantas and R. van Grondelle, *Nat. Phys.*, 2014, **10**, 676–682.
55 A. R. Holzwarth, M. G. Müller, M. Reus, M. Nowaczyk, J. Sander and M. Rögner, *Proc. Natl. Acad. Sci. U. S. A.*, 2006, **103**, 6895–6900.
56 A. Pavlou, J. Jacques, N. Ahmadova, F. Mamedov and S. Styring, *Sci. Rep.*, 2018, **8**, 2837.
57 A. Jha, P.-P. Zhang, V. Tiwari, L. Chen, M. Thorwart, R. J. D. Miller and H.-G. Duan, *Sci. Adv.*, 2024, **10**, eadk1312.
58 E. Betti, P. Saraceno, E. Cignoni, L. Cupellini and B. Mennucci, *J. Phys. Chem. B*, 2024, **128**, 5188–5200.
59 V. I. Novoderezhkin, J. P. Dekker and R. van Grondelle, *Biophys. J.*, 2007, **93**, 1293–1311.

